Moessbauer-effect and Fenske-Hall molecular orbital study of the electronic structure of several trinuclear iron carbonyl clusters

Margaret L. Buhl, Gary J. Long, and James F. O'Brien

Organometallics, **1993**, 12 (2), 283-288• DOI: 10.1021/om00026a011 • Publication Date (Web): 01 May 2002

Mossbauer-Effect and Fenske–Hall Molecular Orbital Study of the Electronic Structure of Several Trinuclear Iron Carbonyl Clusters

Margaret L. Buhl and Gary J. Long*

Department of Chemistry, University of Missouri—Rolla, Rolla, Missouri 65401-0249

James F. O'Brien

Department of Chemistry, Southwest Missouri State University, Springfield, Missouri 65804-0089

Received May 15, 1992

Fenske–Hall molecular orbital calculations have been carried out on the trinuclear carbonyl clusters $Fe_3(CO)_{12}$, $[Fe_3(CO)_{10}CH]^-$, $[Fe_3(CO)_9CCO]^{2-}$, and $[Fe_2Co(CO)_9CCO]^-$, and their Mössbauer spectra have been measured at 78 K. The iron 4s Mulliken atomic population shows the expected increase as the Mössbauer-effect isomer shift decreases. Further, we find an excellent correlation between the observed isomer shift and the sum of the iron 4s population and the effective nuclear charge they experience. A calculation of the electric field gradients at the iron nuclei, based on the Mulliken atomic charges and the iron wave functions derived from the Fenske–Hall molecular orbital calculations, reveals that the valence contribution by far predominates over the lattice contribution to the electric field gradient at the iron-57 nucleus. There is a rather good correlation between the calculated and observed quadrupole splittings in the iron clusters.

Introduction

The Mössbauer-effect spectra of various trinuclear organoiron carbonyl clusters[1-4] have proven very useful in determining the structural and electronic properties[5-7] of $Fe_3(CO)_{12}$ (Figure 1) and its various neutral derivatives.[1,2,8] However, in general there has been less use of Mössbauer spectral parameters to understand the electronic properties of related trinuclear anionic clusters. Our earlier success in understanding the electronic properties of a series of tetranuclear organoiron butterfly clusters[9] has prompted us to undertake Fenske–Hall molecular orbital calculations on $Fe_3(CO)_{12}$ and the series of related trinuclear anionic clusters shown in Figure 1.

The preparation, structure, and reactivity of trinuclear metal carbonyl clusters[1,10,22] have been the subject of many recent studies because they exhibit reactivity at the carbon atom bonded to the three metals.[14,15] Several investigators have noted that the role of surface carbides in heterogeneous catalysis suggests that metal clusters with carbide

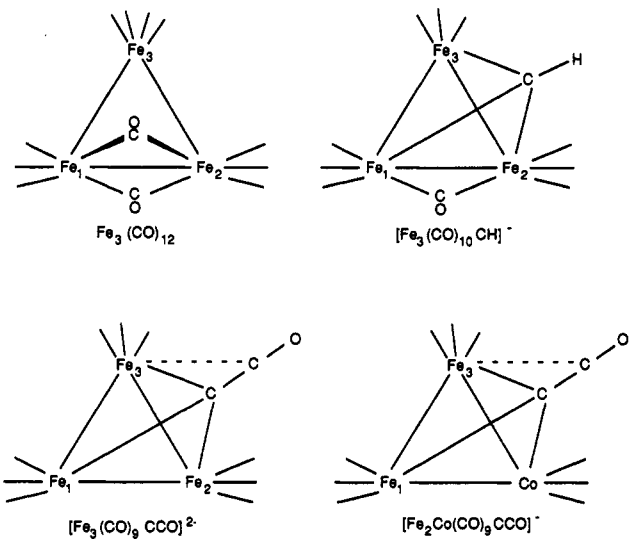

Figure 1. Structures and numbering scheme for the clusters studied herein.

(1) Benson, C. G.; Long, G. J.; Kolis, J. W.; Shriver, D. F. *J. Am. Chem. Soc.* **1985**, *107*, 5297–5298.
(2) Collins, M. P.; Spalding, T. R.; Deeney, F. T.; Longoni, G.; Pergola, R. D.; Venäläinen, T. *J. Organomet. Chem.* **1986**, *317*, 243–253.
(3) Grandjean, F.; Long, G. J.; Benson, C. G.; Russo, U. *Inorg. Chem.* **1988**, *27*, 1524–1529.
(4) Erickson, N. E.; Fairhall, A. W. *Inorg. Chem.* **1965**, *4*, 1320–1322.
(5) Desiderato, R., Jr.; Dobson, G. R. *J. Chem. Educ.* **1982**, *59*, 752–756.
(6) Wei, C. H.; Dahl, L. F. *J. Am. Chem. Soc.* **1969**, *91*, 1351–1361.
(7) Cotton, F. A.; Troup, J. M. *J. Am. Chem. Soc.* **1974**, *96*, 4155–4159.
(8) King, R. B.; Chorghade, G. S.; Bhattacharyya, N. K.; Holt, E. M.; Long, G. J. *J. Organomet. Chem.* **1991**, *411*, 419–430.
(9) Benson, C. G.; Long, G. J.; Bradley, J. S.; Kolis, J. W.; Shriver, D. F. *J. Am. Chem. Soc.* **1986**, *108*, 1898–1903.
(10) Shapley, J. R.; Strickland, D. S.; St. George, G. M.; Churchill, M. R.; Bueno, C. *Organometallics* **1983**, *2*, 185–187.
(11) Barreto, R. D.; Fehlner, T. P.; Hsu, L. Y.; Jan, D. Y.; Shore, S. G. *Inorg. Chem.* **1986**, *25*, 3572–3581.
(12) Wong, K. S.; Haller, K. J.; Dutta, T. K.; Chipman, D. M.; Fehlner, T. P. *Inorg. Chem.* **1982**, *21*, 3197–3202.
(13) DeKock, R. L.; Wong, K. S.; Fehlner, T. P. *Inorg. Chem.* **1982**, *21*, 3203–3209.
(14) Kolis, J. W.; Holt, E. M.; Shriver, D. F. *J. Am. Chem. Soc.* **1983**, *105*, 7307–7313.
(15) Kolis, J. W.; Holt, E. M.; Drezdzon, M.; Whitmire, K. H.; Shriver, D. F. *J. Am. Chem. Soc.* **1982**, *104*, 6134–6135.
(16) Kolis, J. W.; Holt, E. M.; Hriljac, J. A.; Shriver, D. F. *Organometallics* **1984**, *3*, 496–498.
(17) Jensen, M. P.; Sabat, M.; Johnston, D. H.; Jones, L. M.; Shriver, D. F. *J. Organomet. Chem.* **1990**, *383*, 279–294.
(18) Jensen, M. P.; Sabat, M.; Shriver, D. F. *J. Cluster Sci.* **1990**, *1*, 75–91.
(19) Ching, S.; Sabat, M.; Shriver, D. F. *Organometallics* **1989**, *8*, 1047–1058.
(20) Hriljac, J. A.; Shriver, D. F. *J. Am. Chem. Soc.* **1987**, *109*, 6010–6015.
(21) Sailor, M. J.; Brock, C. P.; Shriver, D. F. *J. Am. Chem. Soc.* **1987**, *109*, 6015–6022.
(22) Went, M. J.; Sailor, M. J.; Bogdan, P. L.; Brock, C. P.; Shriver, D. F. *J. Am. Chem. Soc.* **1987**, *109*, 6023–6029.

0276-7333/93/2312-0283$04.00/0

reactivity may play an important part in catalytic processes.[14-16,23-25] Factors believed to play an important role in carbide reactivity are the degree of exposure of the carbon atom,[26-28] the charge on the carbon atom,[27,28] and the "proximity to the HOMO–LUMO gap of molecular orbitals having high carbon-orbital coefficients".[28,29] In order to further understand the bonding in such materials, we have carried out Fenske-Hall molecular orbital calculations on $Fe_3(CO)_{12}$ and the related clusters $[Fe_3(CO)_{10}CH]^-$, $[Fe_3(CO)_9CCO]^{2-}$, and $[Fe_2Co(CO)_9CCO]^-$. Herein we relate the resulting electronic distributions to their structure and confirm these distributions through a comparison of the iron-57 Mössbauer spectral hyperfine parameters of the iron sites.

Experimental Section

X-ray structural results were taken from the literature[7,14-16] and, except for $Fe_3(CO)_{12}$, the crystallographically determined molecular structures were used in the Fenske–Hall calculations. The structure of $Fe_3(CO)_{12}$ was idealized in order to make Fe(1) and Fe(2) symmetry equivalent.[30] However, the asymmetric nature[7] of the bonding between the bridging carbonyl groups and Fe(1) and Fe(2) was retained. The Fenske–Hall calculations,[31] which assume a known, fixed molecular structure, used Herman–Skillman[32] atomic basis functions as modified with the Xα to Slater basis program of Bursten and Fenske[33] and provided with the Fenske–Hall computer code by Prof. M. Hall of Texas A&M University. The double-ζ functions for the 1s and 2s wave functions were reduced to single-ζ functions for these calculations. Ground-state atomic configurations were used for all atoms except for iron and cobalt, for which the assumed $d^{n+1}s^0$ cationic configurations were used. The valence 4s and 4p exponents, provided with the code for the transition-metal atoms, were determined[33] by minimizing the energy difference between the valence eigenvalues obtained from molecular calculations and experimental ionization potentials measured for $M(CO)_6$ and $M'(PF_3)_4$, where M is Cr, Mo, and W and M' is Ni, Pd, and Pt.[34] All Fenske–Hall calculations used the same basis functions, and no effort was made to investigate the influence of changes in these functions on the calculated Mössbauer spectral parameters. A Mulliken population analysis was used to determine the atomic orbital occupancy factors and the atomic charges. These atomic charges were then used to compute[35] the lattice contribution to the electric field gradient at the iron nucleus. The Fenske–Hall-derived iron wave functions were used to compute[35] the valence contribution to the electric field gradient. The total electric field gradient was then calculated and used to compute the quadrupole splitting expected for a given iron site.

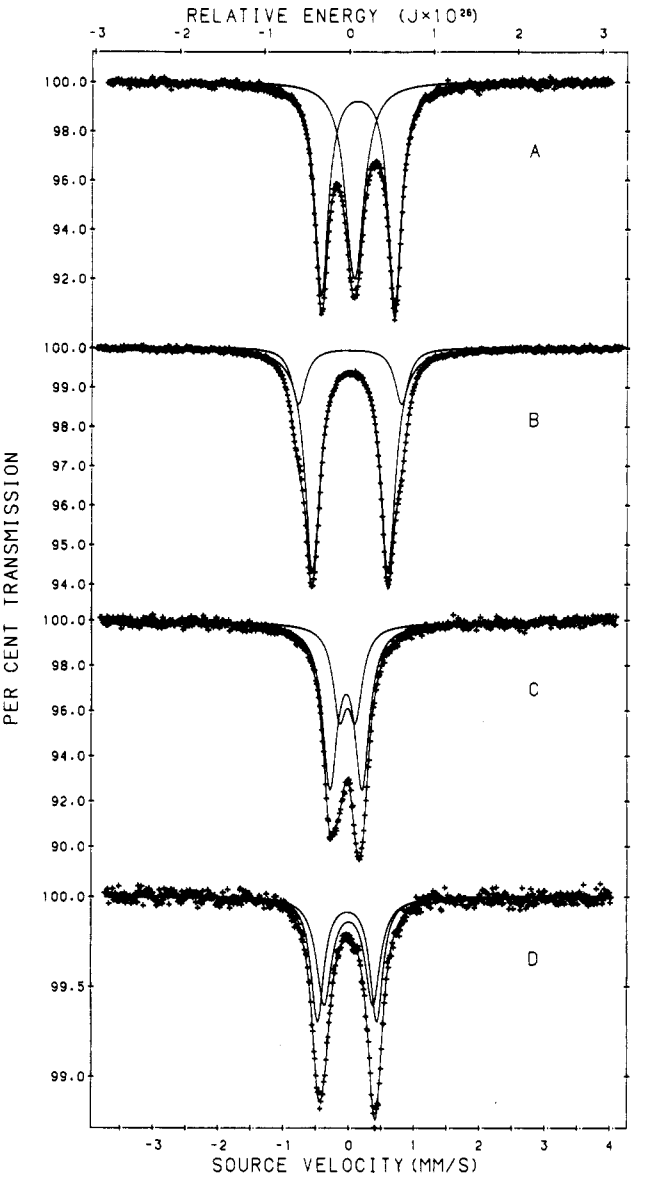

Figure 2. Mössbauer-effect spectra of $Fe_3(CO)_{12}$ (A), $(PPN)[Fe_3(CO)_{10}CH]$ (B), $(PPN)_2[Fe_3(CO)_9CCO]$ (C), and $(PPN)[Fe_2Co(CO)_9CCO]$ (D) obtained at 78 K.

The Mössbauer-effect spectra were measured at 78 K on a constant-acceleration spectrometer which utilized a room-temperature rhodium matrix cobalt-57 source and was calibrated at room temperature with natural α-iron foil. The spectra were fit with two symmetric quadrupole doublets by using standard least-squares minimization techniques. The relative areas of these doublets were constrained to have the values expected on the basis of the known X-ray structures[6,7,14-16] of these compounds. The accuracy of the resulting hyperfine parameters was obtained by using standard error propagation techniques.

Results and Discussion

Mössbauer Spectral Parameters. The Mössbauer-effect spectra of the iron-containing clusters, shown in Figure 1, have been measured at 78 K and the resulting spectra are shown in Figure 2. The spectra have been fit with the minimum number of symmetric quadrupole doublets required to reproduce the spectral line shape. In each case this required two doublets and corresponds to

(23) Beno, M. A.; Williams, J. M.; Tachikawa, M.; Muetterties, E. L. *J. Am. Chem. Soc.* **1980**, *102*, 4542–4544.
(24) Drezdzon, M. A.; Whitmire, K. H.; Bhattacharyya, A. A.; Hsu, W. L.; Nagel, C. C.; Shore, S. G.; Shriver, D. F. *J. Am. Chem. Soc.* **1982**, *104*, 5630–5633.
(25) Muetterties, E. L.; Rhodin, T. N.; Band, E.; Brucker, C. F.; Pretzer, W. R. *Chem. Rev.* **1979**, *79*, 91–137.
(26) Tachikawa, M.; Muetterties, E. L. *J. Am. Chem. Soc.* **1980**, *102*, 4541–4542.
(27) Bradley, J. S.; Ansell, G. B.; Hill, E. W. *J. Am. Chem. Soc.* **1979**, *101*, 7417–7419.
(28) Harris, S.; Bradley, J. S. *Organometallics* **1984**, *3*, 1086–1093.
(29) Kolis, J. W.; Basolo, F.; Shriver, D. F. *J. Am. Chem. Soc.* **1982**, *104*, 5626–5630.
(30) Apparently because of difficulties in solving the disordered structure of $Fe_3(CO)_{12}$, this structure has several highly anisotropic thermal parameters and varying bond distances for the carbonyl ligands.[7] To overcome these atypical structural features, the structure of $Fe_3(CO)_{12}$ was idealized by using the average iron–carbon and carbon–oxygen bond distances.
(31) Hall, M. B.; Fenske, R. F. *Inorg. Chem.* **1972**, *11*, 768–775.
(32) Herman, F.; Skillman, S. *Atomic Structure Calculations*; Prentice-Hall: Englewood Cliffs, NJ, 1963.
(33) (a) Bursten, B. E.; Fenske, R. F. *J. Chem. Phys.* **1977**, *67*, 3138–3145. (b) Bursten, B. E.; Jensen, R. J.; Fenske, R. F. *J. Chem. Phys.* **1978**, *68*, 3320–3321.
(34) See instructions provided with the Fenske–Hall code.
(35) Buhl, M. L. Doctoral Dissertation, University of Missouri—Rolla, 1993.

Table I. Mössbauer-Effect Spectral Parameters[a]

cluster	site	δ	ΔE_Q	Γ	% area
$Fe_3(CO)_{12}$	Fe(1,2)	0.132 (4)	1.119 (6)	0.259 (2)	62 (1)
	Fe(3)	0.076 (4)	0.079 (5)	0.316 (2)	38 (1)
$[PPN][Fe_3(CO)_{10}CH]$	Fe(1,2)	0.002 (3)	1.145 (5)	0.251 (2)	66.7[b]
	Fe(3)	0.001 (4)	1.540 (7)	0.334 (4)	33.3[b]
$[PPN]_2[Fe_3(CO)_9CCO]$	Fe(1,2)	−0.041 (4)	0.494 (2)	0.267 (4)	66.7[b]
	Fe(3)	−0.019 (4)	0.224 (2)	0.253 (6)	33.3[b]
$[PPN][Fe_2Co(CO)_9CCO]$	Fe(1)	−0.019 (4)	0.905 (4)	0.236 (3)	50[b]
	Fe(3)	0.002 (5)	0.746 (5)	0.276 (6)	50[b]

[a] All data in mm/s obtained at 78 K relative to room-temperature natural-abundance α-iron foil. Standard deviations are given in parentheses. [b] Component variable constrained to the given value.

the number of chemically distinct iron sites expected on the basis of the crystal structures of these materials.[6,7,14-16] The component quadrupole doublets are shown in Figure 2, and the resulting hyperfine parameters are given in Table I. The Mössbauer spectra of these clusters are important because the isomer shifts provide information about the varying electron density at the different iron sites in a cluster. Further, the quadrupole splitting provides a measure of the asymmetry of the electronic environment about each iron site. In a preliminary correspondence[1] on the electronic properties of these iron-containing clusters, we reported, on the basis of the relative changes in the isomer shift as $Fe_3(CO)_{12}$ is derivatized to form the anions shown in Figure 1, that the increase in negative anionic charge produced the expected decrease in the isomer shift as a result of increased 4s electron density at the iron nucleus. More specifically, the magnitude of the isomer shift changes indicated that, upon derivatization, the electrons were predominantly localized on the Fe(1,2) sites shown in Figure 1. The derivatization had a much smaller influence on the s-electronic density at the Fe(3) sites.

Fenske–Hall Molecular Orbital Calculations. In order to investigate further the observed changes in the isomer shift upon the formal derivatization of $Fe_3(CO)_{12}$ to form the anions shown in Figure 1, we have carried out Fenske–Hall molecular orbital calculations[31] on these compounds. A summary of the results of these calculations is given in Table II. In carrying out the Fenske–Hall calculations, we have used the transform basis approach described by Housecroft and Fehlner.[36,37] In this method one first optimizes the molecular orbitals for the component "fragments" of the molecules and then combines them to form the entire cluster.

Mössbauer-Effect Isomer Shift. The isomer shift of the iron-57 atom, as obtained from a Mössbauer spectrum, is determined both by the iron 4s orbital population and, to a lesser extent, by the effective nuclear charge, Z_{eff}, experienced by these electrons. Both terms are important because the value of $|\psi_{ns}(0)|^2$ at the nucleus is determined by the number of 4s electrons present on the iron site and their radial distribution. The radial distribution of these electrons is very sensitive to the effective nuclear charge they experience. This effective nuclear charge can be calculated for the iron atoms by using the method of Slater[38,39] or of Clementi and Raimondi[38,40] and the Mulliken atomic orbital populations given in Table II. The two methods of calculating the effective nuclear charge experienced by the iron 4s electrons differ significantly. Slater[38,39] assumed that all of the core electrons shield the valence electrons equally well, thereby ignoring the radial distribution of the shielding electrons. Clementi and Raimondi[38,40] accounted for the difference in the shielding of the valence electrons by the core electrons by calculating the effective nuclear charge from self-consistent-field wave functions. The Slater and Clementi and Raimondi effective nuclear charges for the cluster under study are given in Table II, and the values indicate a significant increase in the effective nuclear charge in the anionic clusters as compared to that in $Fe_3(CO)_{12}$.

It is well-known[41] that, for iron-57, an increase in the iron 4s electronic population will result in a decrease in the observed Mössbauer effect isomer shift. This decrease is illustrated in Figure 3, which plots the isomer shift versus the iron 4s Mulliken atomic population in the clusters shown in Figure 1 and in a series of related homometallic and heterometallic organoiron butterfly clusters and organoiron–copper clusters[9,35,42] for which we have carried out analogous studies. This plot yields a slope of −1.50 mm/s per unit charge, an intercept of 0.53 mm/s, and a correlation coefficient of 0.81. Although the correlation is not ideal, the expected dependence is observed for both the trinuclear iron clusters and a wide variety of related organoiron clusters. A part of the scatter in Figure 3 results from varying effective nuclear charges. As the effective nuclear charge increases, the 4s electron radial distributions contract, the 4s electron density increases at the iron-57 nucleus, and the isomer shift decreases. Hence, the observed isomer shift is a function of both the 4s orbital population and the effective nuclear charge it experiences. This effective nuclear charge is determined predominately by the 3d orbital screening, which of course varies with the 3d orbital population.

It is difficult to know how to weight the influence of the effective nuclear charge, relative to the 4s electron population, in determining the observed isomer shift. However, we have found that the simple sum of the iron 4s Mulliken atomic population and the Slater effective nuclear charge[42,43] provides a correlation with the observed isomer shift. If one uses the more accurate Clementi and Raimondi[38,40] effective nuclear charges, an even better linear correlation is found, as is illustrated in Figure 4 for the trinuclear clusters and several series of related homometallic and heterometallic organoiron butterfly clusters and organoiron–copper clusters.[9,35,42] This plot has a slope of −0.88 mm/s per unit charge, an intercept of 4.47 mm/s, and a correlation coefficient of 0.86 and shows the expected relationship with the isomer shift. The higher the effective nuclear charge experienced by the iron 4s electrons, the higher is the value of $|\psi_{ns}(0)|^2$ at the iron-57 nucleus and the lower is the isomer shift. A comparison of Figure 4 with Figure 3 shows that the effective nuclear charge does make a significant change in the correlation

(36) Housecroft, C. E.; Fehlner, T. P. *Organometallics* **1983**, *2*, 690–692.
(37) Fehlner, T. P.; Housecroft, C. E. *Organometallics* **1984**, *3*, 764–774.
(38) Huheey, J. E. *Inorganic Chemistry*, 3rd ed.; Harper and Row: New York, 1983.
(39) Slater, J. C. *Phys. Rev.* **1930**, *36*, 57–64.
(40) Clementi, E.; Raimondi, D. L. *J. Chem. Phys.* **1963**, *38*, 2686–2689.
(41) Shenoy, G. K. *In Mössbauer Spectroscopy Applied to Inorganic Chemistry*; Long, G. J., Ed.; Plenum Press: New York, 1984; Vol. 1, pp 57–76.
(42) Long, G. J.; O'Brien, J. F. *Hyperfine Interact.* **1988**, *40*, 101–110.
(43) A plot of the Slater effective nuclear charge plus the iron 4s Mulliken atomic population versus the isomer shift yields a linear plot with a negative slope of −0.95 mm/s per unit charge, an intercept of 3.32 mm/s, and a correlation coefficient of 0.65.

Table II. Fenske–Hall Molecular Orbital Results

cluster	site	Mulliken atomic orbital population 3d	4s	4p	Z_{eff}[a]	Z_{eff}[b]	metal charge	total carbonyl charge	ligand	ligand charge	HOMO–LUMO gap
$Fe_3(CO)_{12}$	Fe(1,2)	6.91	0.32	0.89	3.02	4.61	−0.12	0.39			2.37
	Fe(3)	6.87	0.35	0.93	3.03	4.64	−0.15				
$[Fe_3(CO)_{10}CH]^-$	Fe(1)	6.74	0.34	0.97	3.13	4.74	−0.05	−0.44	CH	−0.42	3.97
	Fe(2)	6.77	0.34	0.95	3.12	4.72	−0.05				
	Fe(3)	6.79	0.35	0.90	3.12	4.71	−0.04				
$[Fe_2Co(CO)_9CCO]^-$	Fe(1)	6.73	0.37	0.85	3.18	4.76	0.05	−0.41	CCO	−0.52	3.45
	Co	7.60	0.43	1.17	3.33	5.01	−0.20				
	Fe(3)	6.75	0.35	0.81	3.18	4.75	0.09				
$[Fe_3(CO)_9CCO]^{2-}$	Fe(1)	6.70	0.38	0.92	3.18	4.78	−0.01	−1.37	CCO	−0.64	3.81
	Fe(2)	6.71	0.37	0.91	3.17	4.77	0.00				
	Fe(3)	6.78	0.35	0.86	3.14	4.72	0.02				

[a] Effective nuclear charge, experienced by the metal 4s electrons, calculated by using the method of Slater[38] and the Mulliken atomic populations. [b] Effective nuclear charge, experienced by the metal 4s electrons, calculated by using the method of Clementi and Raimondi[39] and the Mulliken atomic populations.

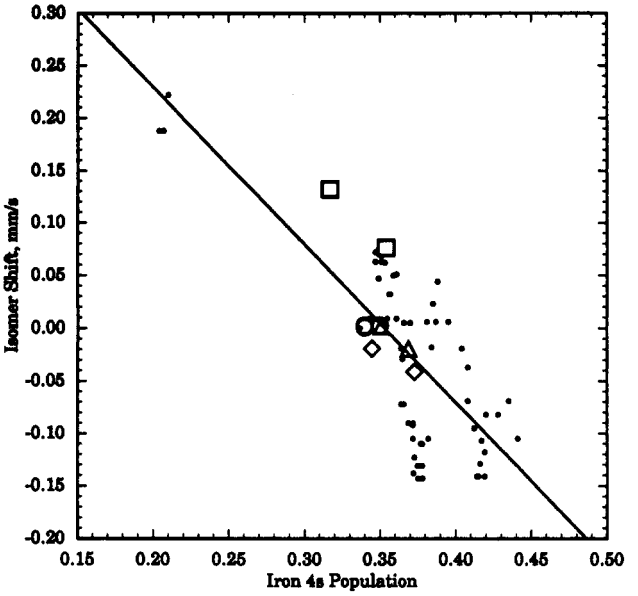

Figure 3. Plot of the Mössbauer-effect isomer shift versus the iron 4s Mulliken atomic population for $Fe_3(CO)_{12}$ (□), $[Fe_3(CO)_{10}CH]^-$ (○), $[Fe_3(CO)_9CCO]^{2-}$ (◇), and $[Fe_2Co(CO)_9CCO]^-$ (△). The small points represent values obtained for a variety of related clusters (see text for references).

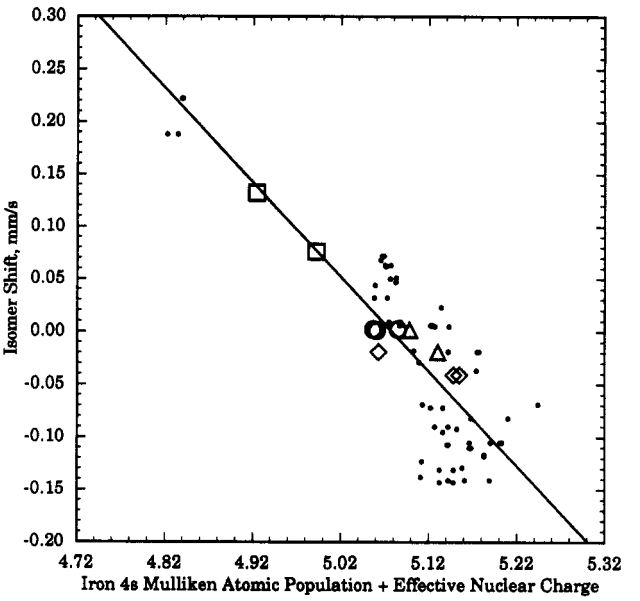

Figure 4. Plot of the Mössbauer-effect isomer shift versus the iron 4s Mulliken atomic population plus the Clementi effective nuclear charge for $Fe_3(CO)_{12}$ (□), $[Fe_3(CO)_{10}CH]^-$ (○), $[Fe_3(CO)_9CCO]^{2-}$ (◇), and $[Fe_2Co(CO)_9CCO]^-$ (△). The small points represent values obtained for a variety of related clusters (see text for references).

with the observed isomer shift, especially for the clusters studied herein. Indeed, the neutral $Fe_3(CO)_{12}$ molecule exhibits the highest isomer shifts and its Fe(3) site, which has the highest 4s electron density, the most negative charge, and a slightly higher effective nuclear charge, has a smaller isomer shift than do the equivalent Fe(1,2) sites with the bridging carbonyl ligands. In the anionic clusters, the Fe(1,2) sites in $[Fe_3(CO)_9CCO]^{2-}$ have the highest 4s electron density, the highest effective nuclear charge, the most positive metal charge, and hence the most negative isomer shift, as shown in Figure 4.

On the basis of an analysis of the changes in the isomer shift upon the derivatization of $Fe_3(CO)_{12}$ to form the remaining clusters, we have previously[1] indicated that, upon derivatization of the cluster, the 4s iron valence electrons are more predominately localized on the Fe(1,2) sites, the derivatization having a much smaller influence on the electronic density of the Fe(3) site. The Fenske–Hall molecular orbital results allow us to test this conclusion. Indeed, as shown in Figure 5, the 4s electron density on the Fe(3) site is virtually constant, whereas the 4s electron density on the Fe(1,2) sites shows a small increase. However, the changes in the 3d and 4p Mulliken orbital populations are much larger and, in general, decrease in the series of clusters. This population decrease results in a decrease in the screening of the 4s electrons, an increase in the effective nuclear charge experienced by the 4s electrons, and a decrease in the isomer shift, as is easily seen in Figure 6. Hence, our original proposal is only true in part, and it seems that the changes in the 4p and especially the 3d orbital populations, through changes in Z_{eff}, are quite important in determining the isomer shift. A similar conclusion[9] was reached earlier for a series of organoiron butterfly clusters. It is interesting that the positive charge on the iron atoms actually increases (see Table II) as the negative charge on the cluster increases.

Mössbauer-Effect Quadrupole Splitting. By using the Fenske–Hall molecular orbital charges and wave functions, it is possible to calculate[35] the electric field gradient at the iron nucleus. This calculation is divided into lattice and valence components. The charges on each of the atoms in the molecule, as determined from a Mulliken population analysis, can be used to calculate the lattice contribution to the electric field gradient at the

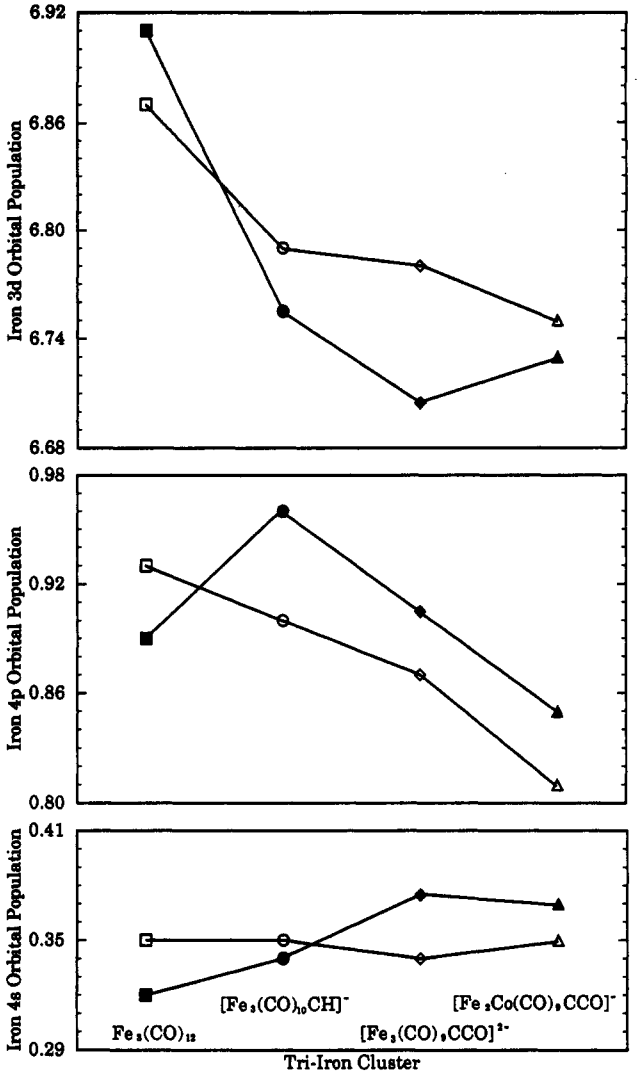

Figure 5. Variation in Mulliken iron atomic orbital populations as a function of the cluster. The closed symbols are Fe(1,2), and the open symbols are Fe(3).

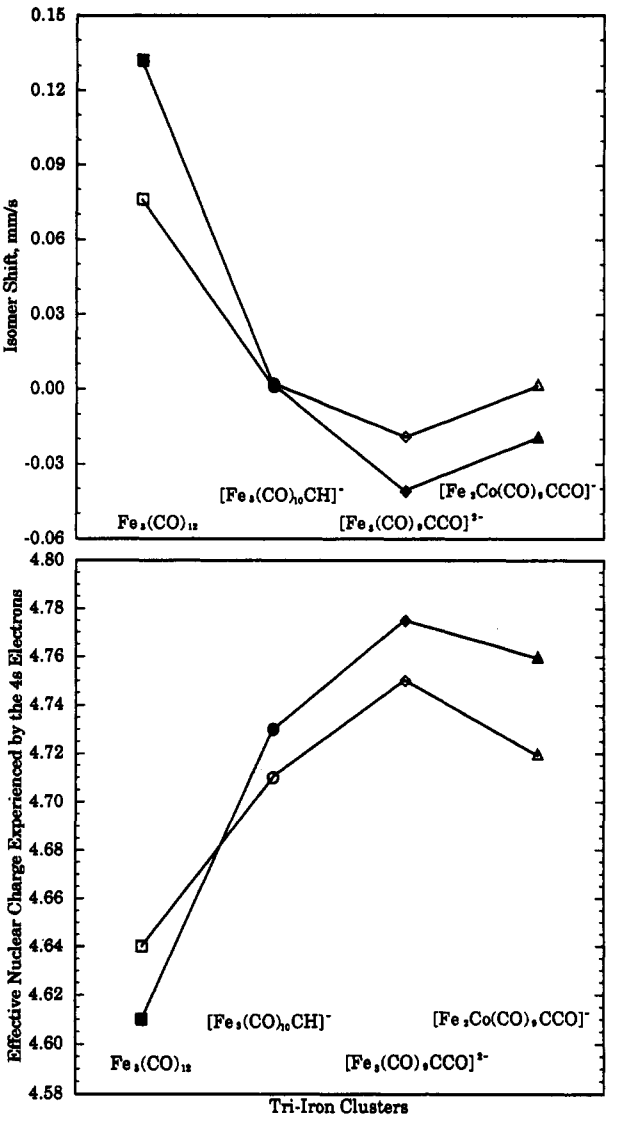

Figure 6. Comparison of the changes in the isomer shift and the Clementi effective nuclear charge experienced by the iron 4s electrons. The closed symbols are Fe(1,2), and the open symbols are Fe(3).

iron nucleus. The coefficients of the occupied orbitals may be used to calculate the valence contribution to the electric field gradient. The results of these calculations, and the corresponding Mössbauer-effect quadrupole splittings, are given in Table III. The experimental and calculated splittings are plotted in Figure 7. In Table III, V_{zz} is the principal component of the EFG tensor, η is the asymmetry parameter, $|V_{xx} - V_{yy}|/|V_{zz}|$, where $|V_{zz}| > |V_{yy}| > |V_{xx}|$, and ΔE_Q is $(eQV_{zz}/2)(1 + \eta^2/3)^{1/2}$, where Q is the iron-57 nuclear quadrupole moment and e is the charge on the proton. In Figure 7 we have used the sign of the calculated V_{zz} value to determine the sign of the observed quadrupole interaction, whose sign cannot be determined from the experimental spectrum. It is immediately apparent from the last column in Table III that the lattice contribution to the EFG is small and that the valence contribution dominates. This indicates that the nonintegral electronic population of the 3d and 4p atomic orbitals in the trinuclear iron clusters (see Table II) is the predominant reason that these clusters have large electric field gradients and, hence, large quadrupole splittings. As indicated in Table III, the lattice contribution is at most 13% for the Fe(1) site in $[Fe_3(CO)_{10}CH]^-$ and is generally less than 10% of the valence contribution to the electric field gradient at the nucleus. As might be expected, in neutral $Fe_3(CO)_{12}$ the lattice contribution to the EFG is at most 1%.

Table III. Comparison of Observed and Calculated Quadrupole Interactions[a]

						valence contribn		
		obsd	calcd					% of
cluster	site	ΔE_Q	ΔE_Q	V_{zz}[b]	η	V_{zz}[b]	η	ΔE_Q
$Fe_3(CO)_{12}$	Fe(1,2)	1.119	−1.93	−8.41	0.82	−8.41	0.82	100
	Fe(3)	0.079	0.97	4.65	0.11	4.61	0.10	99
$[Fe_3(CO)_{10}CH]^-$	Fe(1)	1.145	−1.08	−4.98	0.51	−5.24	0.45	87
	Fe(2)	1.540	−1.49	−6.54	0.76	−6.41	0.86	89
	Fe(3)	1.145	−0.99	−4.49	0.61	−4.47	0.62	98
$[Fe_3(CO)_9CCO]^{2-}$	Fe(1)	0.494	0.80	3.68	0.52	3.92	0.48	93
	Fe(2)	0.494	0.78	3.44	0.74	3.68	0.68	91
	Fe(3)	0.224	−0.44	−2.01	0.54	−2.11	0.44	91
$[Fe_2Co(CO)_9CCO]^-$	Fe(1)	0.905	−1.37	−6.02	0.78	−6.16	0.79	96
	Fe(3)	0.746	−1.22	−5.22	0.89	−5.33	0.91	97

[a] The ΔE_Q values have units of mm/s. The obsrved ΔE_Q values were obtained at 78 K. [b] The V_{zz} values have units of V/m^2 and should be multiplied by 10^{21}.

With the exception of $Fe_3(CO)_{12}$ there is a good correlation between the calculated and observed quadrupole interactions. In general, the calculated quadrupole

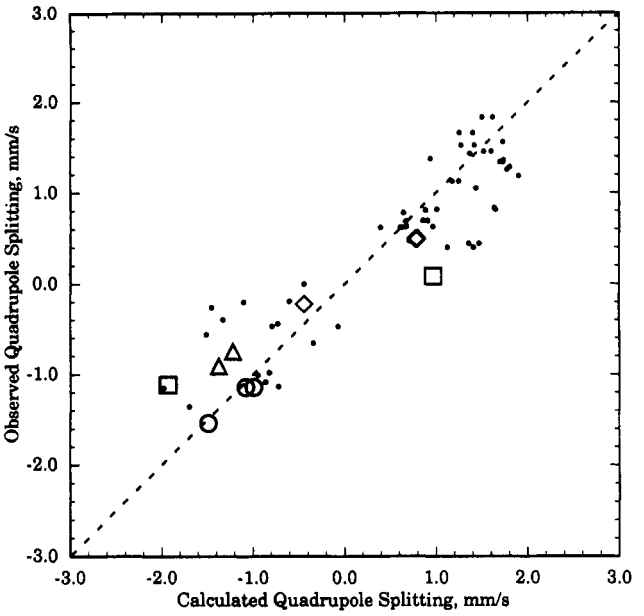

Figure 7. Plot of the observed Mössbauer-effect quadrupole splittings versus the quadrupole splittings obtained from the electric field gradients calculated from the iron molecular orbital wave functions and atomic charges for $Fe_3(CO)_{12}$ (□), $[Fe_3(CO)_{10}CH]^-$ (○), $[Fe_3(CO)_9CCO]^{2-}$ (◇), and $[Fe_2Co(CO)_9CCO]^-$ (△). The small points represent values obtained for a variety of related clusters (see text for references).

interaction is larger in magnitude than the observed splitting. However, it should be noted that differences in the quadrupole splittings at different sites in a given cluster are rather well reproduced by the calculated values. In some instances small differences in the calculated quadrupole interactions are not resolved in the experimental spectra. However, in each such case it was found that equally good or better fits to the experimental spectra could be obtained by adding the expected third doublet.

For $Fe_3(CO)_{12}$, the calculated quadrupole splittings are somewhat larger than the observed splitting. The reason for this difference is not clear at this time, but it should be noted that the difference between the two calculated and the two observed splittings is again quite similar. The experimental temperature dependence[3] of ΔE_Q in $Fe_3(CO)_{12}$ indicates different signs for the quadrupole interactions of the Fe(1,2) and Fe(3) sites. The calculated splittings also have a different sign, but reversed from our earlier[3] assignment. Of all the sites studied, the Fe(3) site in $Fe_3(CO)_{12}$ has the smallest asymmetry parameter, η, indicating that it is the only site with close to axial symmetry. Thus, it appears that the interactions of the methyne and ketenylidene ligands with the Fe(3) site substantially increase, as might be expected, the distortion from axial symmetry at this site. The experimental splittings also show that this site has the largest increase in ΔE_Q and hence decrease in local electronic symmetry upon the formal derivatization of $Fe_3(CO)_{12}$ to form the anions. The results shown in Figure 7 for the trinuclear iron clusters studied herein, and for many related clusters[9,35,42] (see the small data points in Figure 7) indicate that the Fenske–Hall-derived iron valence wave functions are quite adequate, at least to a first approximation, for calculating the electric field gradients at the iron sites in various organoiron clusters.

Acknowledgment. We thank Drs. D. F. Shriver and J. W. Kolis for providing some of the cluster samples, Dr. M. B. Hall for providing the Fenske–Hall computer code, and Drs. T. P. Fehlner, C. E. Housecroft, F. Grandjean, L. Biolsi, and A. Penico for helpful discussions during the course of this work. G.J.L. thanks the donors of the Petroleum Research Fund, administered by the American Chemical Society, for their support of this work.

OM920265P